https://doi.org/10.1595/205651324X17092043851525 *Johnson Matthey Technol. Rev.*, 2024, **68**, (4), 503–520

JOHNSON MATTHEY
TECHNOLOGY REVIEW

technology.matthey.com

Ultrafast Spectroscopy at the Central Laser Facility

Applications to the study of commercially relevant materials

Paul M. Donaldson*, Igor V. Sazanovich, Partha Malakar, Sourav Maiti, Mike Towrie, Gregory M. Greetham§

Central Laser Facility, Research Complex at Harwell, Science and Technology Facilities Council, Rutherford Appleton Laboratory, Harwell Science and Innovation Campus, Didcot OX11 0QX, UK

Email: *paul.donaldson@stfc.ac.uk, §greg.greetham@stfc.ac.uk

PEER REVIEWED

Received 11th December 2023; Revised 28th February 2024; Accepted 29th February 2024; Online 29th February 2024

In this article, we will examine ultrafast spectroscopy techniques and applications, covering time-resolved infrared (TR-IR) spectroscopy, time resolved visible (TA) spectroscopy, two-dimensional infrared (2D-IR) spectroscopy, Kerr-gated Raman spectroscopy, time-resolved Raman and surface sum-frequency generation (SSFG) spectroscopy. In addition to introducing each technique, we will cover some basics, such as what kinds of lasers are used and discuss how these techniques are applied to study a diversity of chemical problems such as photocatalysis, photochemistry, electrocatalysis, battery electrode characterisation, zeolite characterisation and protein structural dynamics.

1. Introduction

There are many techniques of modern optical spectroscopy that are used to great effect across the world of chemistry, materials science and interface areas such as biochemistry and physical chemistry. Standard ultraviolet (UV), visible to near-IR, fluorescence, IR and Raman instruments occupy important roles in many laboratories for quantitative molecular concentration analysis, species identification and species characterisation. The concepts and instrumentation around these techniques were established long ago, yet the continuous development of new spectroscopic techniques and applications keeps the field both relevant and exciting. For instance, it is now possible to measure spectra with laser pulses that are million billionths of a second, i.e. femtoseconds in duration. These techniques of ultrafast spectroscopy in their many forms are the subject of this article and encompass many different possibilities. Here we will discuss techniques which take advantage of the time resolution of spectroscopy possible with ultrafast lasers, where spectra can be acquired from femtoseconds to seconds in a single measurement. With short laser pulses it is possible to rapidly trigger changes in a sample and to observe transient chemical species, charge carriers, excited vibrations, temperature changes or perturbations of charge density on the timescale of the laser pulse. As short laser pulses can be, momentarily extremely bright, these effects can be large enough to be manipulated by further laser pulses. Ultrafast spectroscopy can be as much about the possibilities of these high peak intensities as it is about time resolution.

Ultrafast spectroscopy is a very broad area. The cost of the equipment required and the research intensive nature of developing techniques and applications mean that it is typically carried out in specialised academic research laboratories. At the Science and Technology Facilities Council (STFC) Rutherford Appleton Laboratory's Central Laser Facility (CLF), a strategy for lowering the

technical barriers to scientists accessing ultrafast spectroscopy has long been in place. This is to offer ultrafast spectroscopy to academic and industrial users through facility instruments and trained staff on a science campus where the provision of facilities is at the heart of the operational ethos of every laboratory. The CLF's ultrafast spectroscopy facility is called 'ULTRA' and benefits from being collocated with numerous other laser facilities at CLF, the neutron beamlines at the ISIS spallation source, X-ray beamlines at the diamond light source synchrotron and satellite test facilities at RAL Space.

This article will reveal the breadth of ultrafast spectroscopy by discussing the different techniques and applications offered by the ULTRA facility. Historically, the approach of providing ultrafast spectroscopy facilities at the CLF first took shape in the 1980s with the provision of UV lasers for Raman spectroscopy (1) and in the 1990s with the provision of time-resolved Raman and UV-visible absorption facilities (2, 3). Over this period, ultrafast IR laser (4) and IR array detector technology (5) significantly improved. The addition of TR-IR spectroscopy and Kerr-gated Raman spectroscopy in the 2000s in the form of the 'PIRATE' facility (6) significantly broadened the kinds of chemical problems tackled with time resolved spectroscopy at the CLF. Increased demand and improvements in technology resulted in ultrafast IR and Raman facility provision expanded and diversified from 2005 onwards through the development of the 'ULTRA' laser system (7), followed in 2016 by the LIFEtime laser system (8, 9). Many of the applications described in this article originate from the ULTRA laser system (7) which made its final pulses of light in August 2023 in order to be replaced by a new set of CLF-ULTRA instruments which, as part of the 'HiLUX' project, are based on next-generation laser and detector technology (10) and set to begin coming online in 2025.

2. Ultrafast Time Resolved Spectroscopy: The Fundamentals

Most techniques of ultrafast time-resolved spectroscopy require multiple laser beams to be focussed at a sample and for selected laser beams or emission to be directed towards a detector for analysis. **Figure 1** shows schematically different focussing arrangements for the approaches discussed in this paper. With the appropriate laser light sources to hand (see Section 3), ultrafast time-resolved spectrometers draw heavily on the techniques of modern optics for the manipulation of the light sources, for the creation of optimal conditions for irradiating a sample and for the various means of determining the spectrum of the light. **Figure 2** breaks the process down into several important technological steps: control of the timing of the laser pulses, generation of a spectrum of the laser pulses or emission and detection of the laser pulses.

Control of laser timing down to femtosecond precision can be achieved simply by varying the path length that a laser beam travels over using a translation stage. The practical limit is how much length can be accurately added and removed on demand without changing any characteristics of the laser beam such as divergence or pointing. For example, the CLF LIFEtime instrument uses a

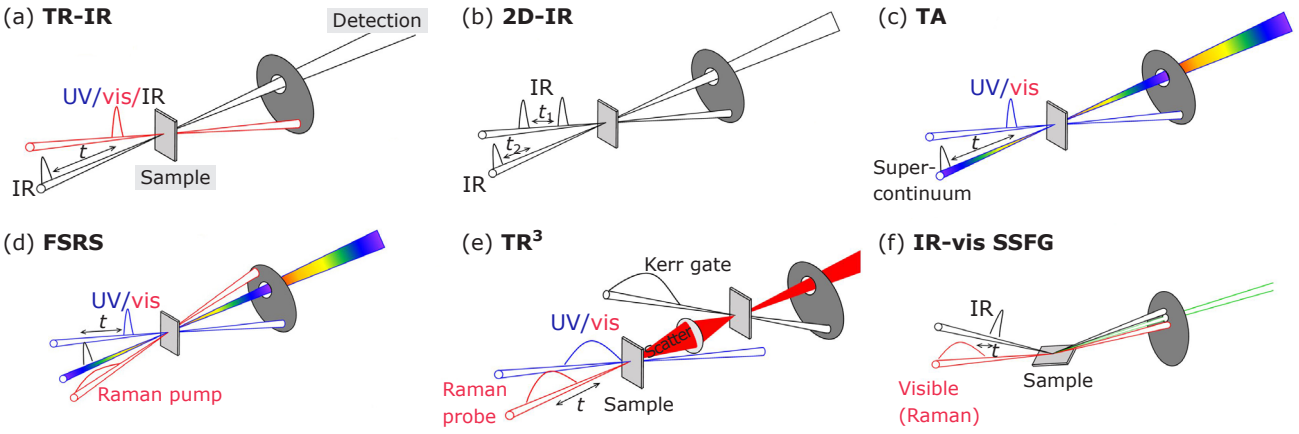

Fig. 1. Example laser beam configurations for ultrafast spectroscopy: (a) TR-IR with UV-visible-IR pumping; (b) 2D-IR; (c) TA (transient visible absorption spectroscopy); (d) FSRS; (e) Kerr-gated TR^3; (f) IR-visible SSFG

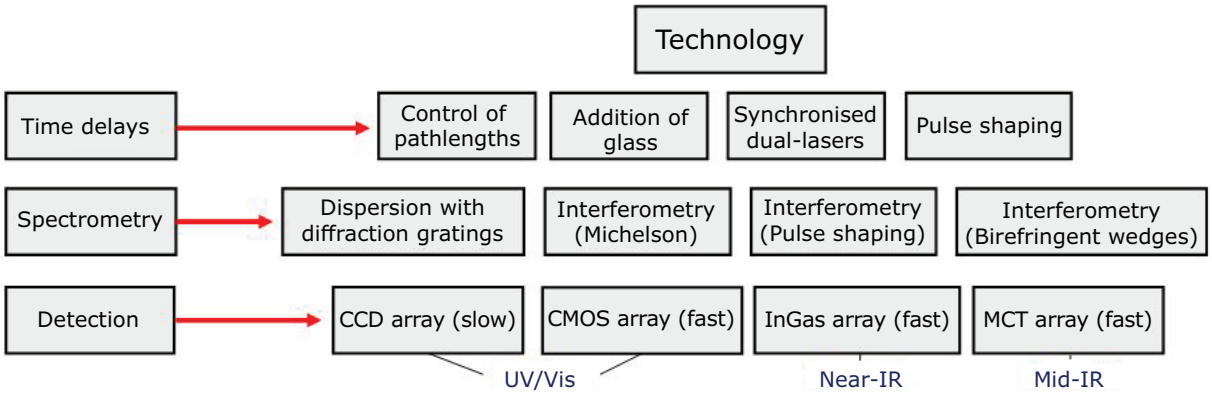

Fig. 2. Technology for controlling optical time delays, for spectrometry and for light detection in ultrafast spectroscopy

two-pass, 1.2 m long translation stage, with a precision of 1 µm, to achieve a tuneable delay of up to 16 ns at a precision of 12 fs. To achieve longer delays between laser pulses, the approach of electronically synchronising one laser source to another, with adjustable timing is used (11, 12). Other routes to changing time delays in the range of tens of picoseconds and less include the addition of glass, sometimes in the form of scanned wedges (13), or the use of a device called a pulse shaper (14). Pulse shaping not only enables a pulse delay to be changed, it also enables the generation of pairs of pulses with adjustable delay. This makes interferometry possible as a means of recovering a spectrum: another technological requirement in a spectroscopy setup. In comparison with a conventional Michelson or Mach-Zender interferometer, or the interesting approach of using birefringent wedges for interferometry (15, 16), pulse shaping is by far the fastest approach, with arbitrary pulse timing changes at 100 kHz rates possible (9, 17). Even faster is the standard approach for recovering a spectrum of a laser pulse in time resolved spectroscopy: to disperse the laser pulse in a spectrograph onto a 'fast' array detector, detecting every point of the spectrum for every single laser shot. It is this approach that is preferable for all techniques where at least a single frequency axis is required. For multidimensional spectroscopy, in order to recover a further frequency axis, interferometry or pulse shaping must additionally be used.

3. Ultrafast Time Resolved Spectroscopy: The Lasers

Ultrafast time resolved spectroscopy is enabled by ultrafast laser technology. We provide a general overview of commonly used light sources in **Figure 3**. Most ultrafast lasers (defined as generating femtosecond to picosecond pulses) rely on a mode-locked 'oscillator' laser, which by design emits short pulses of light at rates of up to 100 MHz. These are often too weak to use for time-resolved spectroscopy or for non-linear wavelength conversion, so are used to 'seed' an amplifier system, giving fixed visible or near IR (NIR) wavelengths of much higher energy pulses at lower rates of 1 kHz to 1 MHz. The CLF-ULTRA A and B systems are based on titanium:sapphire oscillator and amplifier technology operating at 10 kHz (7). The CLF-ULTRA's LIFEtime system is based on ytterbium:KGW laser technology, which can operate efficiently at higher rates than titanium:sapphire lasers (8–10).

Supercontinuum, also known as white light generation, is a process where the intense, relatively monochromatic light from an amplifier becomes polychromatic when focussed through glasses, optical fibres or gases. Visible supercontinuum light is a common form of ultrafast probe light (and occasionally pump light) for time-resolved visible spectroscopy. Supercontinuum IR light is low in the amount of energy per unit spectrum, but successfully used as an ultrafast probe in numerous TR-IR and 2D-IR experiments (18). In order to gain tuneable laser light across the UV, visible and IR with the required energy for ultrafast spectroscopy, one further device called an optical parametric amplifier (OPA) is required (5). These must be pumped by titanium or ytterbium amplifiers as described above. OPAs often rely on the phenomenon of supercontinuum generation for generating broadband light to act as a seed source. Generating enough spectral 'bandwidth' is one key challenge for OPAs. For

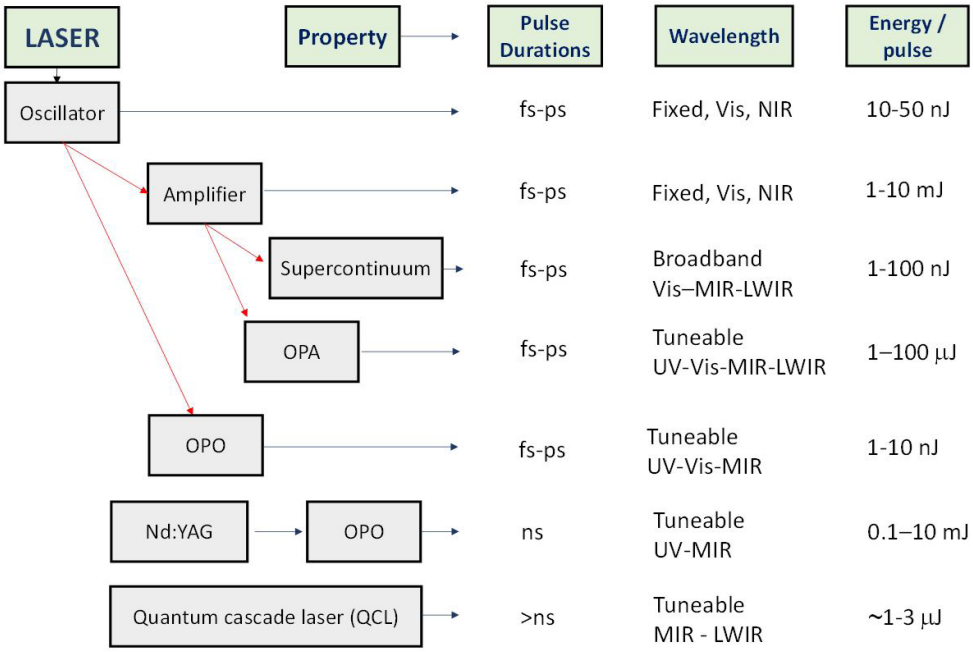

Fig. 3. Some common laser types, system nomenclature and typical pulse parameters for ultrafast time resolved spectroscopy. OPA, OPO, MIR = mid-IR, LWIR = long-wavelength IR

example, the more bandwidth a laser pulse has, the more spectrum can be probed without tuning the centre wavelength. IR OPAs pumped by 40–100 fs pulses give light that is anywhere from 100 cm^{-1} to 500 cm^{-1} in bandwidth (4, 7, 8, 19), with 1000 cm^{-1} the largest to date (20) (full width at half maximum). The direct driving of an optical parametric oscillator (OPO) with a laser oscillator also results in a broadly tuneable source. Transient spectroscopy imaging with the low resulting pulse energies is possible when the light is used with the tight focussing conditions of a microscope (21, 22).

There are many compact nanosecond lasers available, operating across the visible and IR. **Figure 3** therefore includes the common arrangement of using an neodymium:YAG laser in combination with an OPO to obtain broadly tuneable light across the visible and IR and the quantum cascade laser (QCL), which makes light across the IR.

4. Time Resolved Infrared Spectroscopy (UV-Visible Excitation)

We begin our discussion of time resolved spectroscopy techniques with time resolved IR spectroscopy combined with UV-visible excitation (TR-IR, **Figure 1(a)**). Here, a pulse of UV-visible light creates transient populations of excited states and an IR pulse then tracks subsequent relaxation, chemistry and molecular dynamics through vibrational spectroscopy. Chemical reactions occur over many timescales. Examples include: (i) femtosecond charge migration; (ii) picosecond and nanosecond relaxation of electronic and vibrational states and local structural changes; (iii) microsecond and millisecond diffusion rate-limited interactions or structural dynamics in large biomolecular systems; and (iv) millisecond to second physical diffusion through sample solvents and matrices. CLF-ULTRA gains access to all of these timescales on one instrument using a version of TR-IR called time resolved multiple probe spectroscopy (TRMPS) (8, 23). Here, two laser amplifiers are synchronised and the optical and electronic delay scheme enables femtosecond to microsecond timing between the excitation and probing light pulses. Longer timescales are accessed through further probe pulses, one after another. With a probing repetition rate of 100 kHz (8), the LIFEtime facility at CLF-ULTRA acquires an IR spectrum every 10 μs. At an excitation rate of 10 Hz for example, LIFEtime will acquire 10,000 IR spectra spanning a 100 ms timescale, extending the femtosecond to microsecond kinetics observed by the first probe pulse.

Both single probe-pulse TR-IR and TR-IR using the TRMPS approach at CLF-ULTRA see ever-increasing applications in the study of the physical and chemical properties of materials in excited electronic states.

Which to use depends on the timescales sought, the repetition rate of the laser system used, the signal-to-noise required and the rate at which a sample can be excited and re-excited. High repetition rate probe lasers and adjustable rate pump lasers for TRMPS is becoming our preferred solution (10). Single probe-pulse TR-IR has nevertheless been widely applied at CLF-ULTRA in studies ranging from fundamental bimolecular reactions in solution (24, 25), in biomolecules tracking charge transfer through proteins (26), in the excited state dynamics of photoactive proteins (27, 28), relationships between electronic excited states and DNA damage in solution (29–31) and crystals (32).

The TRMPS TR-IR technique has provided insights into the steps underpinning photocatalytic reaction cycles, helping the search for catalysts using earth abundant non-toxic metals and the search for metal-free catalysts. Some examples include new understanding of manganese catalysed reactions, where picoseconds to hundreds of microseconds TRMPS TR-IR spectroscopy allowed the direct observation of bond formation in important intermediate reaction steps (33, 34), the study of hydrogen evolution from dye sensitised photocathodes and novel dye-based sensitisers (35, 36).

An example of manganese catalysed photochemistry is the search for new routes to convert nitrogen into useful chemicals. In certain living organisms this is mediated by the nitrogenase enzyme, which has a molybdenum-based active site. Taking inspiration from nature, a new class of manganese-based compounds that provide insight into the interaction of nitrogen with transition metals were studied by TRMPS TR-IR at CLF-LIFEtime by Lynam and co-workers (37). **Figure 4** provides an example of a TR-IR measurement of one such system in heptane plus dissolved nitrogen or argon, spiked with trace amounts of water. The TR-IR measurements shown in **Figure 4(b)**–**4(d)** track the dynamics of the parent compound (**Figure 4(a)** blue squares) and its excited state evolution into either adducts of heptane (**Figure 4(a)** blue circles), nitrogen (**Figure 4(b)** red triangles) or water (**Figure 4(b)** green hexagons, from trace amounts in the solvent). On 355 nm excitation, within picoseconds' the complex with heptane forms (**Figure 4(b)**) and by 500 ns

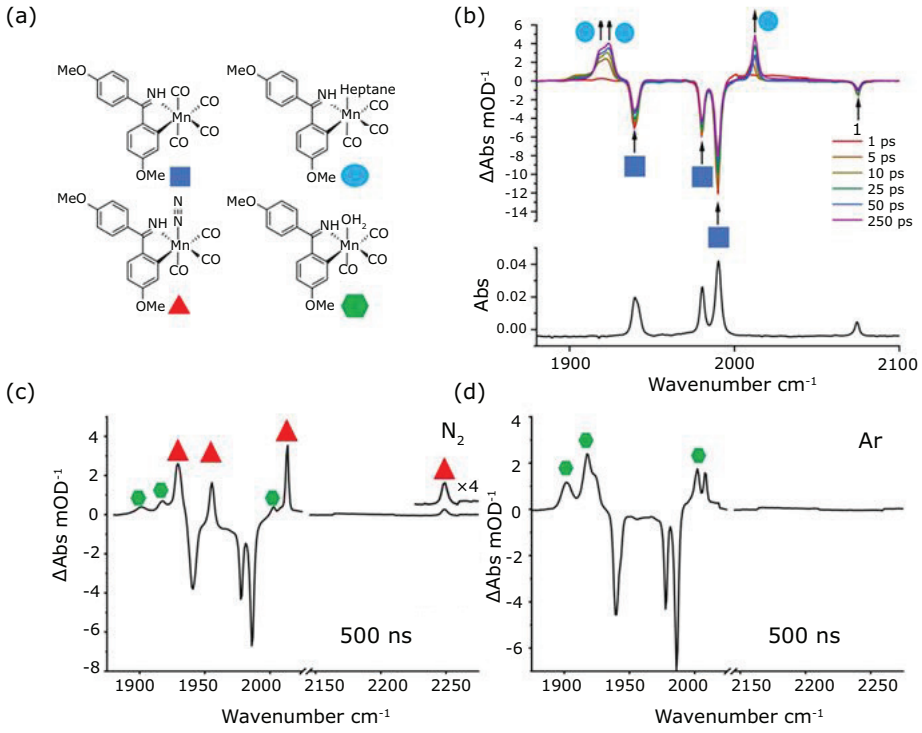

Fig. 4. Carbonyl region TR-IR follows the binding of ligands to: (a) Mn complexes, shown with a blue square. The colour and shape coded adducts that form after photoexcitation with 355 nm light and carbon monoxide loss are also shown; (b) with heptane as the solvent, the TR-IR spectrum shows that the heptane adduct forms first. Adducts of other species present in the solvent form on a 500 ns timescale: (c) the competitive binding of nitrogen in the TR-IR spectrum with water (present in trace amounts); (d) replacement of nitrogen with argon reveals the IR spectrum of the water adduct

the system has in the presence of nitrogen either become a mixture of nitrogen complex and water complex (**Figure 4(c)**), or just the water complex in the presence of argon (**Figure 4(d)**), demonstrating competitive binding between nitrogen and water.

New classes of photocatalysts using a process termed photoredox-catalysed atom transfer radical polymerisation (ATRP) are emerging for the controlled synthesis of polymers. In the development of these catalysts, emphasis has been placed on triplet rather than singlet state excited systems, where the longer lifetime of triplet states and lower likelihood for back electron transfer suggests they would be more effective than singlet state photocatalysts. TR-IR was recently used by Orr-Ewing and co-workers in a study of the singlet and triplet excited state dynamics of organic ATPR catalysis challenging this idea (38). The same authors also applied TR-IR to photochemical decarboxylation of carboxylic acids as a route to generation of intermediates for chemical synthesis using metal free catalysts. TRMPS TR-IR tracked the decarboxylation of cyclohexanecarboxylic acid on the picosecond to microsecond timescale and confirmed the formation of reactive carboxyl radicals as a reaction intermediate (39).

The final application example in this section we share are in-house studies of proton conduction mechanisms in protic ionic liquids using the pH jump method with TRMPS TR-IR, as shown in **Figure 5** (40). Here, a photoacid is added to a proton conducting ionic liquid. The release of protons is triggered by a short visible pulse of light. IR spectroscopy follows the protonation state of both the photoacid and the solvent, with the fast (picoseconds) deprotonation and long (hundreds of nanoseconds) recovery of the system accessed through the TRMPS approaches at CLF-ULTRA. For the ionic liquid examined, study of the full photocycle enabled elucidation of a vehicular proton transfer mechanism.

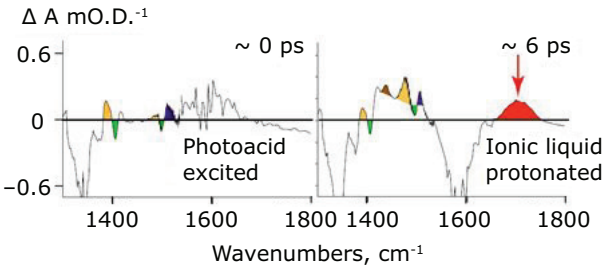

Fig. 5. The transfer of protons from a photoacid (HPTS) to a protic ionic liquid solvent (ethyl ammonium formate) is observed by TR-IR to occur in picoseconds. TR-IR detects the excited photoacid at 0 ps (coloured bands) and the formation of the protonated formate (formic acid, shown in red at 1720 cm^{-1}) and deprotonated photoacid by 6 ps. The approach, as well as a detailed study of the entire photocycle is described in reference (40)

5. Time Resolved Infrared Spectroscopy (Infrared Excitation)

5.1 Infrared-pump- Infrared probe and T-Jump spectroscopy

When the UV-visible excitation of the TR-IR experiment is replaced with IR excitation (**Figure 1(a)**), we have a form of pump-probe spectroscopy dealing purely with the behaviour of excited vibrational modes. Vibrational pump-probe spectroscopy is one step from 2D-IR spectroscopy (next section) and can measure excited vibrational lifetimes, as well as the rotational dynamics of a molecule through the anisotropy decay calculated from time-dependent polarised pump-probe spectra (41). We currently use this approach to quantify the dynamics of different types of water in the proton exchange membrane Nafion™. IR pump-probe signals vary as the square of the molar absorption coefficient and it is possible to combine IR absorption strengths and pump-probe signal strengths to enable calculation of concentrations or absorption strengths without recourse to Beer-Lambert titrations (42).

Laser excitation can be used to rapidly heat a sample and then combined with laser spectroscopy to probe the sample with high time resolution. This is known as temperature jump (T-jump) spectroscopy (43). IR excitation is less damaging compared with visible excitation and does not require addition of visible absorber, such is the strong IR absorption of most samples. At CLF-ULTRA, IR-excitation T-jump spectroscopy (43) has been used to study the unfolding of proteins, DNA and RNA (44). The possibility of using T-jump spectroscopy to heat zeolites by up to a hundred degrees and study the evolution of heated adsorbates from nanoseconds to seconds was recently realised (45). The technique is currently being developed to enable studies of fast thermally activated chemistry and desorption and diffusion processes in zeolites.

5.2 Two Dimensional-Infrared Spectroscopy

2D-IR spectroscopy is an IR pump-probe measurement where the effect of both the probe laser frequency and the pump laser frequency on the pump-probe signal are resolved (46). This results in a 2D spectrum in a similar way to how multi-pulse nuclear magnetic resonance (NMR) achieves a 2D-NMR spectrum. What additional information is gained? If we think about a single 'one dimensional' IR absorption band as having a frequency, a line shape and an amplitude, the equivalent band in a 2D-IR spectrum appears as a peak pair where we gain a measure of the frequency of the second excited state and a 2D line shape that visually reports on molecular mechanisms giving rise to the line shape. Vibrational modes which couple to one another, exchange energy or even interconvert through structural dynamics give cross peaks in the off-diagonal regions of the spectrum. As a time-resolved method, 2D-IR spectroscopy can quantify dynamics and rotational motions that influence vibrational frequencies or intensities over the course of an excited vibrational mode's lifetime. As a pump-probe method, 2D-IR spectroscopy can be used in conjunction with IR absorption spectroscopy to determine concentrations and transition strengths, leaving behind the requirement for a Beer-Lambert-style titration (42).

Figure 1(b) shows the most common optical approach for measuring a 2D-IR spectrum, where interferometry recovers the pump frequency response and spectral dispersion with array detection recovers the probe frequency response. 2D-IR has developed from the late 1990s with a strong emphasis on studying biomolecules and water solvation dynamics (47–50). CLF-ULTRA plays an active role in making 2D-IR accessible, in improving the technique (9, 10, 51) and supporting a user community with applications such as developing analysis methods for quantifying proteins in serum (52), assessing ligand-DNA binding (53), understanding cation dynamics in perovskites (54), understanding the IR spectra of polarons in supramolecular assemblies (55) and quantifying hydrogen bond dynamics in a protic ionic liquid (56). 2D spectroscopy has also been extended at CLF-ULTRA by developing methods for measuring 2D-IR-Raman spectra (51). Selective excitation of specific vibrational modes was applied to excited state dynamics at CLF-ULTRA by the group of Weinstein, who excited bridging ligands in a platinum based organometallic donor-acceptor complex with IR light in order to perturb electron transfer initiated by a visible pulse (57). The sequence of electronic excitation (UV), selective IR excitation and then IR probing to monitor the electron transfer is known as transient 2D-IR spectroscopy (46).

The technology required for successful applications of 2D-IR to surfaces and solids has recently begun to develop. Application to surface adsorbed molecules in the attenuated total reflectance (ATR) has been demonstrated (59). Application to heterogeneous solids such as bassanite to measure water dynamics (60) and zeolites to observe water cluster structure (61) are significant advances for the technique, but also require the dispersion of the sample in an index matching mull to reduce the effects of intense scattered pump-light interfering with the measurement. CLF-ULTRA have recently developed an approach that enables 2D-IR spectra to be measured from pressed pellets of sample in transmission, demonstrating recovery of high quality 2D-IR spectra of P25 titania, pyrogenic silica and zeolites (58) Forthcoming publications will examine hydrogen bonding in pyrogenic silica (62), silanol nest defects in ZSM-5 and water in several zeolites. The application of 2D-IR spectroscopy to zeolites is a new endeavour, with much left to learn about what the spectra report on. **Figure 6** concludes this section by showing a recent 2D-IR spectrum collected from our laboratory of deuterated zeolite Y's ν(OD) stretch band. Marked in the spectrum are tentative assignments of a cross peak due to bound water **A**, the highly

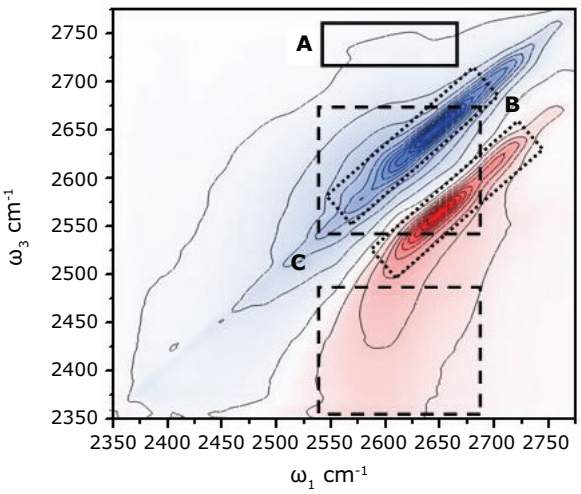

Fig. 6. A 2D-IR spectrum of deuterated zeolite Y in the ν(OD) stretch region collected as described in reference (58)

elliptical shape of an inhomogeneously broadened, non-hydrogen bonded distribution of Brønsted sites **B** and **C** a broader distribution of Brønsted sites or silanol defects which are interacting weakly with hydrogen bond acceptors.

6. Time Resolved Visible Spectroscopy (UV-Visible Excitation)

Time-resolved visible spectroscopy is a powerful approach for studying light activated processes. Also known as transient absorption (TA) spectroscopy, TA techniques excite photo-responsive systems with a selected wavelength range of UV or visible light and probe the response with broadband UV-visible-NIR light that is spectrally resolved on an array detector. For TA spectroscopy, silicon and InGaAs array detectors are used to accurately determine the spectral intensity of the probe light transmitted through the photo-excited sample. Due to the high intrinsic quantum efficiency of the silicon and InGaAs array detectors used, as well as visible detection being far more widespread than for mid-IR, UV-visible detection systems are cheaper, more compact, more sophisticated and much simpler to use than the mid-IR analogues required for TR-IR.

Examples of how excitation and probing pulses can be generated for TA are described in **Figure 3**. TA is the visible analogue of TR-IR (Section 4), but more widespread than TR-IR due to the laser and detection technology in the visible part of the spectrum being simpler, visible absorption spectroscopy itself being more common and time resolved visible spectroscopy being highly relevant in the study of solar devices, light emission materials, photocatalysts and photosynthesis. There are facilities at universities which offer various versions of TA spectroscopy. CLF-ULTRA specialises in offering the TRMPS technique (23) for TA measurements alongside TR-IR, which enables measurements from femtoseconds to seconds with a single sample without the need to understand variations in pump fluences between different instruments.

Recent examples of TRMPS TA work from the CLF-ULTRA user programme on biomolecule photochemistry include the measurement in multi-heme proteins of the oxygen photodissociation and rebinding (63) and the rate of electron transfer from dye to heme (64) and heme-to-heme (65). TA has also been used to study the behaviour of dyes for biological super-resolution imaging (66) and the perturbation of excited state dynamics of a ruthenium complex by site specific binding to i–motif DNA structures (67). The study of solar cell materials is also a common application of the CLF-ULTRA TA setups (68).

In pH-jump experiments as described in **Figure 5** of Section 4, whereas TR-IR spectroscopy can study both the photoacid and the protonated solvent, TA tracks the evolution of the UV-visible absorbing photoacid. For the case of TR-IR, spectral congestion means that in elucidating proton transport mechanisms (40), the response of the photoacid had to be recovered by fitting procedures whereas in TA, the electronic absorption of the photoacid states can be studied in isolation. **Figure 7(a)** shows the TA colormap of the HPTS photo-acid in water after 390 nm excitation and **Figure 7(b)** shows an example of the kinetic evolution of the excited photoacid, indicating formation of the excited state ROH* as a bleach of the spectrum and the subsequent formation of the deprotonated state RO^{*-} as an induced absorption. At this point, the solvating water has become protonated. When the RO^{*-} relaxes to the ground state, the proton is recovered from the water to reform ROH. This TA data was collected on a TA spectrometer implemented on the LIFEtime system (8) and serves to show the wide time range (hundreds of femtoseconds to microseconds) accessible with the TRMPS technique from a single measurement.

7. Kerr-Gated Raman Spectroscopy

Raman spectroscopy is a vibrational spectroscopy technique which operates in the spectral range from UV to NIR, most often in the visible. The Raman technique measures inelastic scattering by molecular vibrations of sample-incident photons (usually in the visible spectral range). Raman is governed by different selection rules to those of IR spectroscopy, one of several properties making it complementary to IR. As the Raman effect is essentially a scattering effect, it is often the technique of choice for those working with scattering or non-transmissive materials, for example inhomogeneous catalysts or battery materials.

When the incident light's wavelength is far from the electronic absorption of a sample, such an experiment condition is termed 'non-resonant Raman'. When the incident light's wavelength falls within the electronic absorption band of the sample, Raman scattering is enhanced by many orders of magnitude (termed 'resonance Raman').

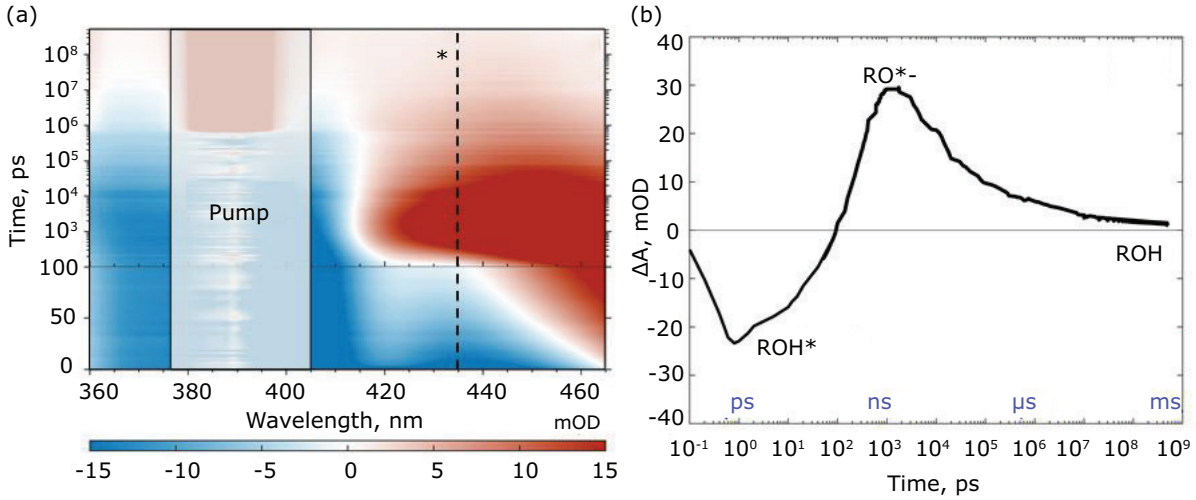

Fig. 7. 100 kHz TRMPS-TA with 1 kHz, 390 nm pumping: (a) a photoacid (HPTS) dissolved in water is excited and the transient response is probed across 360–460 nm; (b) shows the response at 435 nm (marked * in (a)). The photoacid states are ROH (ground state), ROH* (excited state) and RO*$^-$ (deprotonated)

Here, vibrations coupled to the electronic transition are enhanced. Resonance Raman spectroscopy is therefore a powerful technique for identifying reaction coordinates, i.e. the vibrations associated with a particular electronic process.

The main factors affecting signal intensity in Raman spectroscopy are the intrinsic polarisability of the molecule associated with each vibrational mode and the frequency of incident light ω. In non-resonant Raman the intensity of scattering increases as ω^4. Many materials of interest are fluorescent or have some fluorescent impurities. As Raman scattering is an inherently weak effect, the quantum yield of impurity fluorescence normally exceeds the Raman scattering efficiency by many orders of magnitude and under resonance probing conditions, fluorescence most likely spectrally overlaps Raman signal, making Raman investigations impossible. Fitting and subsequently subtracting the fluorescence background from the raw data is rarely an option, as fluorescence intensity fluctuates in square-root proportion to its size (known as shot noise). This noise, which increases as the fluorescence intensity increases overwhelms the weak Raman signal.

Over the last few decades, a number of approaches have been devised to circumvent the fluorescence background problem in Raman experiments. Two options are to use either NIR or UV Raman probe wavelengths, so as not to induce fluorescence (NIR) or to avoid it spectrally overlapping with Raman (UV). Switching to NIR Raman inevitably leads to losing resonance enhancement and Raman cross-section (ω^4 law). Raman in the UV is challenging due to the limitations of optics transmission, difficulties of generating narrow-band UV light and losing transition or species selectivity due to many species or transitions being in resonance with the UV probe beam.

Other options for circumventing fluorescence are shifted Raman excitation (69) and temporal gating (70). The shifted excitation Raman approach still results in the full amount of fluorescence being recorded by the detector. For the case of strong fluorescence the shot noise can still obscure the weak Raman signal. Temporal gating is superior in this respect, as it prevents most of the fluorescence from even being detected. The most efficient temporal gating approach so far is optical Kerr-gating. Kerr-gated Raman spectroscopy was suggested in mid-1980s (71) and implemented at the CLF in late 1990s (72). Kerr-gated Raman offers picosecond time resolution, superior fluorescence rejection and provides flexibility in Raman probe wavelength. The approach can be readily configured to record Raman spectra of transiently generated excited states, enabling time-resolved Raman and time-resolved resonance Raman (known as TR^3), covered in the next section.

The general concept of Kerr-gated Raman spectroscopy is shown in **Figure 1(e)**. The optical Kerr effect is defined as induced birefringence in a polarisable material caused by an intense electric field, for example from a high-peak-power laser pulse. Bearing in mind that a birefringent material acts on polarised light to rotate its polarisation, an optical Kerr-gate comprises two crossed polarisers and the Kerr medium in-between, which serves

to transiently allow transmission of light through the polarisers only when the intense picosecond Kerr-gating laser pulse induces the birefringence. If Raman scattering is generated from a separate picosecond laser pulse, it can be collected and passed through the gate at precisely the right moment for transmission. Fluorescence usually occurs on greater than nanosecond timescales and does not pass through the gate efficiently. **Figure 8** shows the diagram of the Kerr-gated Raman setup currently in operation at CLF.

A number of materials with high polarisability can be used to achieve Kerr-gating. For applications in Raman spectroscopy, our material of choice is carbon disulfide, which offers a wide spectral window (*ca*. 380 nm to NIR) and high gating efficiency (>50% transmission). For Kerr-gated Raman in the UV, we use benzene as the Kerr medium which extends the spectral detection window down to *ca*. 300 nm at the expense of gating efficiency.

Since its first implementation in the late 1990s, the Kerr-gated Raman facility at CLF has been used extensively to enable Raman studies of highly emissive samples in both ground and excited electronic states. We first discuss examples of using the Kerr-gated Raman technique to study challenging materials in the ground electronic state. Excited state studies are discussed in the following section.

Zeolites are widely used in the chemical industry as catalysts for heterogeneous catalysis. Catalytic stability is a challenge when using zeolites on an industrial scale. Carbon deposits formed during reaction lead to deactivation of the catalyst. It is challenging to monitor the many intermediate carbon species under reaction conditions. Using conventional Raman spectroscopy is typically prevented because of the strong intrinsic fluorescence of zeolites and reaction intermediates. Recently, Beale and co-workers published a comprehensive *operando* study of methanol conversion in zeolites using the Kerr-gated Raman technique implemented at CLF-ULTRA (73). Kerr-gated Raman enabled high-quality Raman data to be recorded from the catalyst under *operando* conditions by suppressing the strong fluorescence. The authors were able to follow the formation of hydrocarbon species in several zeolite topologies at various stages of methanol conversion and identified polyenes as crucial intermediates towards formation of polycyclic-aromatic hydrocarbons.

Another notable example of a Kerr-gated Raman application comes from the area of lithium-ion battery research. Monitoring lithiation of the graphitic carbon anodes of batteries with optical techniques presents significant challenges, as they are typically non-transparent materials absorbing across a broad spectral range. Raman spectroscopy is one of the very few techniques applicable for this purpose, however at high lithiation stages a strong background fluorescence emanates from the graphitic carbon electrode, restricting the use of conventional Raman spectroscopy to low lithiation studies. Hardwick and co-workers recently employed the Kerr-gated Raman capability at ULTRA-CLF to circumvent that problem and follow Raman band positions of a graphitic carbon electrode *operando* while cycling the lithium battery cell across the full range of charge (74). The authors demonstrated that the broad graphitic band originally located at 1590 cm^{-1} for $Li_{0.5}C_6$ gradually shifts over the course of lithiation to 1564 cm^{-1} for lithiated graphite. The Raman band position dependence on the lithiation stage of lithium battery cell can therefore be used as a diagnostic tool to control the lithiation stage of charge of graphitic carbon negative electrodes.

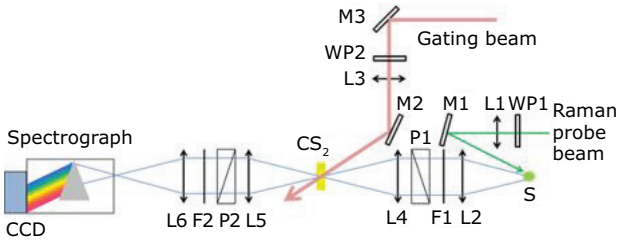

Fig. 8. Optical layout for Kerr-gated Raman. S = sample, WP1 and WP2 = half waveplates, L1 to L6 = lenses, M1 to M3 = beam delivery mirrors, F1 and F2 = long-pass and short-pass filters, P1 and P2 = polarisers, CS_2 = the Kerr cell filled with carbon disulfide

8. Time Resolved Raman Spectroscopy

Among the range of time-resolved vibrational techniques offered by CLF-ULTRA, TR^3 and femtosecond stimulated Raman scattering (FSRS) are those capable of providing Raman data from electronic excited states with (ultra) fast time resolution.

TR^3 technique is an extra capability used with Kerr-gated Raman. The general concept is very similar to that illustrated in the previous section in **Figure 8**. In addition to the Raman probe beam focussed at the sample, an extra pulsed laser beam is delivered to the sample to excite the sample

(known as the actinic pump). The wavelength of the actinic pump is chosen to match the electronic transition of interest, while the Raman probe beam wavelength is matched with the resonance of the sample in the electronic excited state. The time delay between the actinic pump and the Raman probe pulses can be adjusted to probe the signal at a particular stage of evolution of the excited species with picosecond time resolution. Although it is not the optical Kerr-gating that provides the key capability of taking time-resolved Raman data, but rather the interaction of the actinic pump and Raman probe pulses with the sample, as the majority of the materials under study are emissive in the excited state, optical Kerr-gating is necessary for distinguishing the weaker Raman signal from the fluorescence background.

TR^3 spectroscopy has a diverse range of applications, from investigating fundamental photochemical reactions to studying processes and reactions immediately relevant to real-world problems, such as photocatalyst development. Work by Cowan and co-workers is an example of the latter (75). Here the authors studied one of the most active linear polymer photocatalysts for hydrogen production, poly dibenzo[*b,d*]thiophene sulfone (P10). The underlying mechanism giving the high efficiency of this organic photocatalyst was not fully understood until recently. TA measurements gave ambiguous data due to a number of broad, overlapping UV-visible bands. In contrast, TR^3 spectroscopy could probe directly the vibrational signatures of short-lived excitations, simplifying their assignment. Utilising the TR^3 technique, Cowan and co-workers identified polaron-pair formation before the thermalisation of the initially populated excited states as an important factor in generating the long-lived photoelectrons that provide the photocatalytic activity.

Femtosecond stimulated Raman spectroscopy (FSRS) is an alternative approach for bringing ultrafast time resolution into Raman spectroscopy. As the wording in the name of the technique suggests, FSRS is not a spontaneous Raman technique like Kerr-gated Raman or TR^3 but stimulated. This is achieved by inducing ('stimulating') the Raman signal to be emitted by the sample with the help of a bright, broadband ultrafast laser pulse coinciding in time with the narrower Raman pulse. The narrow-band pulse, which is termed 'Raman probe' in spontaneous Raman applications (like Kerr-gated Raman or TR^3) is termed 'Raman pump' in the FSRS experiments.

The layout of FSRS experiment (**Figure 1(d)**) has much in common with the TA spectroscopy experiment of **Figure 1(c)** described in Section 6. Similar to time-resolved visible spectroscopy, the sample is first excited with an actinic pump pulse, which in FSRS is between tens to hundreds of femtoseconds in duration. In most cases, white light supercontinuum acts as the stimulating beam. When the spatially overlapped Raman pump and broad-band probe pulses coincide in time at the sample, the bright broad-band probe beam stimulates the emission of Raman light from the sample. This approach provides significantly higher intensity of Raman signal over spontaneous Raman. The time resolution is defined by the femtosecond actinic pump and white light probe pulses and yet the practical spectral resolution of the recorded Raman signal is defined by the narrow-band Raman pump pulse. The Raman pump pulse can be spectrally tuned to match the excited-state absorption of the sample, which provides selectivity towards excited state Raman over the ground state Raman.

As an illustration of FSRS applications at CLF-ULTRA, we mention the work of Heyes and collaborators, who studied the organic photovoltaic material polymer and fullerene heterojunction (76). FSRS revealed extremely fast polaron formation within 300 fs of excitation. With the charge of the newly generated polaron carriers expected to significantly perturb the polymer framework, surprisingly, no conformational changes were detected in the Raman spectrum of the polymer modes on any time scale up to 50 ps, contrary to expectations. This was interpreted as an indication that the charge pairs created in that polymer on photoexcitation do not interact strongly with one another.

9. Surface Sum Frequency Spectroscopy

Vibrational spectroscopy of surfaces and molecules at surfaces is important in many areas of catalysis and materials science. Techniques such as reflection-absorption IR (RAIRS), surface enhanced IR (SEIRA) and surface enhanced Raman spectroscopy (SERS) can all measure spectra from the small numbers of molecules at interfaces. 2D-IR spectroscopy (59) and near-field IR with atomic force microscopy have also reached monolayer sensitivity. SSFG (77) occupies a unique place amongst these techniques. With SSFG it is possible to obtain vibrational spectra of buried interfaces without interference from bulk molecules and

without requiring any form of surface enhancement nanostructures for the adsorbate molecules.

SSFG light is generated by focussing IR and visible laser beams at a surface. For examining buried interfaces, the laser light must not be significantly absorbed by the bulk medium in which the interface is buried. SSFG light is emitted from the sample at the sum of the IR and visible frequencies (**Figure 1(f)**) as a directional beam of similar divergence properties to the visible and IR beams. SSFG emission is very weak and when performed with broadband femtosecond IR pulses uses a visible spectrograph and sensitive charge-coupled device (CCD) camera for detection similar to Raman spectroscopy. SSFG combines IR light to drive molecular vibrations and visible light to drive Raman polarisation on the same vibration simultaneously, giving a net charge oscillation and therefore light emission at the sum of IR and visible frequencies. Similar to Raman spectroscopy, to obtain a vibrational spectrum in frequency or wavenumber units, the visible laser frequency used in SSFG is subtracted from the SSFG emission spectrum. The visible pulse must therefore be narrow in spectral width (greater than picosecond duration). The IR pulse can be broadband (50–300 fs) to give SSFG that can be dispersed as a spectrum onto a multi-pixel array detector, or narrowband (greater than picosecond), measured by a single detector and tuned in frequency to give SSFG spectrum.

As both an IR and a Raman process are involved in SSFG, vibrations must be both IR and Raman active to be observable. Symmetric molecules cannot generate vibrational SSFG light. For non-symmetric molecules, the SSFG process is interesting in the sense that the phase of the light emitted depends on the orientation of the molecules. The bright lasers used to detect the weak SSFG emission from molecules in the laser focus induce the molecules to emit SSFG signal collectively with a well-defined relative phase. Such coherent emission means that there can be interference between different SSFG sources, whether considered as individual molecules, collections of molecules or multiple interfaces. An important example of this is in bulk solution, where the random orientation of molecules (and consequent SSFG optical phase) results in total destructive interference of the different SSFG sources and hence no emitted SSFG signal.

Two scenarios where cancellation of SSFG emission does not occur is for molecular crystals lacking inversion symmetry and for molecules at interfaces. The symmetry breaking at a single interface means that there are no molecules emitting opposite-phase SFG fields. Note that if the interface molecules are randomly oriented and the vibrational frequency is independent of each molecule's orientation, there will be no SSFG signal from the surface. The molecules probed should also only be on one surface in the laser beams, as additional interfaces give their own SSFG emission which interfere with the others. For example, SSFG from identical molecules on the opposite faces of a material much thinner than the wavelength of SFG light may cancel, as would SSFG from molecules on the surfaces of porous solids at random orientations.

At CLF-ULTRA, SSFG was applied by the group of Cowan and co-workers in some of the first ever studies of transition metal electrocatalysts under potentiostatic control (78, 79). In these works, both the ligand carbonyl stretch mode of the catalysts and the CN stretch of the acetonitrile solvent were SSFG active and their behaviour during redox cycles of several transition metal CO_2 reduction catalysts were observed. SSFG was able to clearly follow the formation of the intermediates at the electrode in synchrony with cyclic voltammetry and to observe spectral differences providing information regarding catalytic intermediate identity, structure and mechanism at the electrode surface. Following these studies, SSFG applications to electrocatalysis were recently reviewed by the Cowan group (77).

Figure 9 shows two SSFG spectra of the CN stretch bands of a monolayer of $NH_4^+SCN^-$ deposited on gold and collected using the SSFG spectrometer at CLF-ULTRA. We will use these spectra to understand several concepts in SSFG spectroscopy. These are the difference between homodyne and heterodyne measurements and the appearance of the non-resonant background signal present in homodyne measurements, which we discuss first. If there are no molecular vibrations driven by the IR laser pulse, SSFG spectra will nevertheless contain a wavelength independent emission from there always being a charge density change at an interface. Charge in matter is polarisable at any frequency of light and so the visible and IR fields cause interfacial charge density to weakly oscillate at the sum-frequency component. This 'nonresonant background' is apparent for the gold surface of **Figure 9(a)** and spans the spectral width of the laser pulse used to generate the SSFG spectrum (~400 cm^{-1} full width at half height). Being more polarisable, metal surfaces tend to have stronger SSFG non-resonant backgrounds than dielectric materials. For SSFG from vibrations

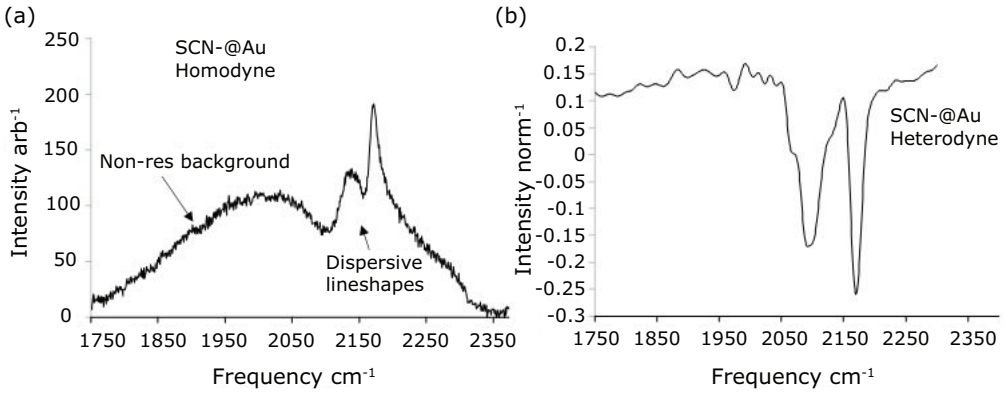

Fig. 9. (a) Homodyne; (b) heterodyne SSFG spectra of the SCN stretch bands of a monolayer formed from immersion of bare gold in aqueous ammonium thiocyanate. This data was collected using CLF-ULTRA's SSFG spectrometers

resonant with the IR light, the vibrationally resonant SSFG field is emitted 90° phase shifted relative to the non-resonant background. We will discuss the consequence of this phase shift shortly. We turn to the concepts of homodyne and heterodyne SSFG.

With absorption of photons being the common means of discussing absorption of light, it often comes as a surprise that treating light classically (as electric fields) can yield an accurate and powerful framework for understanding and computing light-matter interactions such as light absorption in molecular spectroscopy. In this picture, for IR or visible absorption measurements, the relatively bright light (field) used to determine the absorption of a sample generates a weak field from the molecule's vibrations or electronic transitions in the sample proportional to their concentration and transition strength. This field is out of phase with the brighter incident light source. The incident light source illuminates the detector, as does the weaker emission. In this picture their interference gives rise to the observed attenuation of light at the detector. Light intensity is proportional to the square of the total electric field, so after subtracting the intensity spectrum of the incident light source, the dominant contribution to an IR or visible absorption spectrum are the interference terms between the bright 'reference' field and weak molecule fields. These are the peaks in an IR or UV-visible absorption spectrum. These peaks point in one direction only from the baseline: positive when in absorbance units. They are often referred to as 'absorptive' peaks. This would seem trivial, but if the phase relationship between the bright reference field and the weak emission were to change somehow, the interference could become part-destructive, part-constructive. A part-positive, part-negative peak-shape in a spectrum is referred to as 'dispersive'. The interference of the non-resonant background with the out-of-phase vibrationally resonant bands in **Figure 9(a)** shows this effect clearly. An example of deviations from absorptive peaks in a time resolved IR absorption measurement is described by Donaldson *et al.* (80). The weak emission of IR light through an optically excited IR absorbing sample is normally overlapped with the incident light (**Figure 1(a)**). In reference (80) it is isolated from the incident IR light source by arranging an optically excited sample to be in the pattern of a grating. The weak emission is the IR light diffracted from the grating which can be sent to a detector and interfered with a separate reference source.

The process of using a separate reference source in spectroscopy to detect a weak field is called 'heterodyne' detection. In this sense, a transmission absorption measurement is a heterodyne measurement where the incident light source acts as the reference source, often called a 'local oscillator'. For SSFG as depicted in **Figure 1(f)**, the light beams used to generate the signal are at a different frequency to the SSFG signal and cannot generate any detectable interference with the SSFG signal. This scenario is often called 'homodyne' detection. With no strong field to interfere with and give rise to the absorptive terms, SSFG signals that are spectrally overlapping can interfere with one another and the non-resonant background instead, giving line shapes with a dispersive component. Dispersive features are twin-peaked and broader than absorptive features. This is undesirable, as it makes it more likely that vibrational features overlap and harder to determine what the

vibrational resonance frequency is. The purpose of heterodyne SSFG spectroscopy is to achieve spectra with the well-behaved characteristics of absorption signals and eliminate the non-resonant background from the spectrum entirely.

Other negative consequences of homodyne SSFG are that the signal strength is quadratic with concentration and that the information regarding which direction a molecule points (encoded in the phase of the SSFG field) is lost. The homodyne SSFG intensity is the square of the field at the detector, so homodyne SSFG is always positive-valued and although the amplitude is largest if the vibrational transition points perpendicular to the interface, it cannot be known whether the molecule points towards or away from the interface, despite the SSFG fields being different to one another in phase by 180 degrees. By interfering the SSFG signal with a reference field (as occurs in heterodyne detection), the phase of the SSFG signal is deduced from the sign of the interference, recovering the sensitivity to molecular orientation.

A downside of heterodyne SSFG is that a more complicated optical arrangement than **Figure 1(f)** is required to generate a stable reference field that efficiently interferes with the SSFG signals. Shown in **Figure 9(b)** is the heterodyne spectrum of the same sample as the homodyne SSFG spectrum in **Figure 9(a)**: a monolayer of $NH_4^+SCN^-$ deposited on gold collected using the SSFG spectrometer at CLF-ULTRA, measured using a heterodyne arrangement similar to that of Petersen (81). It is not easy to know the number of peaks in the spectrum from the homodyne measurement of **Figure 9(a)** without further knowledge of what modes and species should be present. The heterodyne spectrum shows that the system simply contains two negative going CN stretch bands, corresponding either to binding being both at the sulfur and nitrogen ends of the molecule (with the two binding configurations having different frequency), or perhaps two modes of dimerised SCN^- $(NCSSCN)^{2-}$. The fact that both bands are negative indicates the latter as the more likely explanation.

11. Conclusions and Outlook

This article has examined the most common ultrafast spectroscopy techniques available to the user community at CLF-ULTRA, presented some of the science of CLF-ULTRA's user community and provided an overview of ultrafast spectroscopy techniques relevant to chemistry, catalysis, energy storage and materials science. The techniques and instrumentation at CLF-ULTRA are developing rapidly and we see many exciting opportunities for new science using new high-signal-to-noise TRMPS spectrometers delivering the best IR and visible transient spectroscopy, new methods for obtaining 2D-IR spectra and Kerr-gated Raman spectra of scattering heterogeneous catalysts such as zeolites, new methods for rapidly initiating chemical reactions with T-jump spectroscopy and for obtaining surface molecule spectra with SSFG. Though we have left out any discussions of imaging, this can be applied to any of the techniques explored in this article. We see imaging in the near and far-fields as another frontier area of time resolved spectroscopy research both on the instrument and applications side of development.

CLF-ULTRA and indeed all STFC facilities welcome all enquiries about becoming a facility user. We hope that this review article will help newcomers to the field understand some of the plethora of time-resolved spectroscopy techniques and inspire new applications of time-resolved spectroscopy in new areas.

Acknowledgements

The authors thank all users of the CLF-ULTRA facility over the years for bringing the facility to life with great science, collaboration and friendship. The upcoming new HiLUX facility is gratefully acknowledged as a UKRI infrastructure investment. We would also like to thank STFC and BBSRC for both funding the Ultra A, B and LIFEtime systems (LIFEtime: BBSRC, grant Alert 13BB/L014335/1, Ultra A: BBSRC and STFC Joint Facility Grant (ST/501784) and Ultra A TRMPS: STFC. ST/H001840/1). We thank the UKRI Research Complex at Harwell for support in hosting the facility. Paul Donaldson thanks UKRI for UKRI-FLF funding (Grant No. MR/S015574/1) and CLF for access to the laser facility through programme grant LSF1828.

References

1. R. Wilbrandt, W. E. L. Grossman, P. M. Killough, J. E. Bennett, R. E. Hester, *J. Phys. Chem.*, 1984, **88**, (24), 5964
2. P. Matousek, A. W. Parker, W. T. Toner, M. Towrie, D. L. A. de Faria, R. E. Hester, J. N. Moore, *Chem. Phys. Lett.*, 1995, **237**, (3–4), 373
3. I. K. Lednev, T.-Q. Ye, P. Matousek, M. Towrie, P. Foggi, F. V. R. Neuwahl, S. Umapathy, R. E. Hester,

J. N. Moore, *Chem. Phys. Lett.*, 1998, **290**, (1–3), 68

4. R. A. Kaindl, M. Wurm, K. Reimann, P. Hamm, A. M. Weiner, M. Woerner, *J. Opt. Soc. Am. B*, 2000, **17**, (12), 2086
5. P. Hamm, S. Wiemann, M. Zurek, W. Zinth, *Opt. Lett.*, 1994, **19**, (20), 1642
6. M. Towrie, D. C. Grills, J. Dyer, J. A. Weinstein, P. Matousek, R. Barton, P. D. Bailey, N. Subramaniam, W. M. Kwok, C. Ma, D. Phillips, A. W. Parker, M. W. George, *Appl. Spectrosc.*, 2003, **57**, (4), 367
7. G. M. Greetham, P. Burgos, Q. Cao, I. P. Clark, P. S. Codd, R. C. Farrow, M. W. George, M. Kogimtzis, P. Matousek, A. W. Parker, M. R. Pollard, D. A. Robinson, Z.-J. Xin, M. Towrie, *Appl. Spectrosc.*, 2010, **64**, (12), 1311
8. G. M. Greetham, P. M. Donaldson, C. Nation, I. V. Sazanovich, I. P. Clark, D. J. Shaw, A. W. Parker, M. Towrie, *Appl. Spectrosc.*, 2016, **70**, (4), 645
9. P. M. Donaldson, G. M. Greetham, D. J. Shaw, A. W. Parker, M. Towrie, *J. Phys. Chem. A*, 2018, **122**, (3), 780
10. P. M. Donaldson, G. M. Greetham, C. T. Middleton, B. M. Luther, M. T. Zanni, P. Hamm, A. T. Krummel, *Acc. Chem. Res.*, 2023, **56**, (15), 2062
11. M. Towrie, A. Gabrielsson, P. Matousek, A. W. Parker, A. M. B. Rodriguez, A. Vlček, *Appl. Spectrosc.*, 2005, **59**, (4), 467
12. J. Bredenbeck, J. Helbing, P. Hamm, *Rev. Sci. Instrum.*, 2004, **75**, (11), 4462
13. F. Ding, P. Mukherjee, M. T. Zanni, *Opt. Lett.*, 2006, **31**, (19), 2918
14. S.-H. Shim, M. T. Zanni, *Phys. Chem. Chem. Phys.*, 2009, **11**, (5), 748
15. J. Réhault, M. Maiuri, A. Oriana, G. Cerullo, *Rev. Sci. Instrum.*, 2014, **85**, (12), 123107
16. J. Réhault, M. Maiuri, C. Manzoni, D. Brida, J. Helbing, G. Cerullo, *Opt. Express*, 2014, **22**, (8), 9063
17. B. M. Luther, K. M. Tracy, M. Gerrity, S. Brown, A. T. Krummel, *Opt. Express*, 2016, **24**, (4), 4117
18. P. B. Petersen, A. Tokmakoff, *Opt. Lett.*, 2010, **35**, (12), 1962
19. R. Budriūnas, K. Jurkus, M. Vengris, A. Varanavičius, *Opt. Express*, 2022, **30**, (8), 13009
20. J. H. Hack, N. H. C. Lewis, W. B. Carpenter, A. Tokmakoff, *Opt. Lett.*, 2023, **48**, (4), 960
21. N. Gross, C. T. Kuhs, B. Ostovar, W.-Y. Chiang, K. S. Wilson, T. S. Volek, Z. M. Faitz, C. C. Carlin, J. A. Dionne, M. T. Zanni, M. Gruebele, S. T. Roberts, S. Link, C. F. Landes, *J. Phys. Chem. C*, 2023, **127**, (30), 14557
22. Y. Zhu, J.-X. Cheng, *J. Chem. Phys*., 2020, **152**, (2), 020901
23. G. M. Greetham, D. Sole, I. P. Clark, A. W. Parker, M. R. Pollard, M. Towrie, *Rev. Sci. Instrum.*, 2012, **83**, (10), 103107
24. D. R. Glowacki, R. A. Rose, S. J. Greaves, A. J. Orr-Ewing, J. N. Harvey, *Nat. Chem.*, 2011, **3**, (11), 850
25. S. J. Greaves, R. A. Rose, T. A. A. Oliver, D. R. Glowacki, M. N. R. Ashfold, J. N. Harvey, I. P. Clark, G. M. Greetham, A. W. Parker, M. Towrie, A. J. Orr-Ewing, *Science*, 2011, **331**, (6023), 1423
26. C. Shih, A. K. Museth, M. Abrahamsson, A. M. Blanco-Rodriguez, A. J. Di Bilio, J. Sudhamsu, B. R. Crane, K. L. Ronayne, M. Towrie, A. Vlček, J. H. Richards, J. R. Winkler, H. B. Gray, *Science*, 2008, **320**, (5884), 1760
27. L. M. Uriarte, R. Vitale, S. Niziński, K. Hadjidemetriou, N. Zala, A. Lukacs, G. M. Greetham, I. V. Sazanovich, M. Weik, C. Ruckebusch, S. R. Meech, M. Sliwa, *J. Phys. Chem. Lett.*, 2022, **13**, (5), 1194
28. S. P. Laptenok, A. A. Gil, C. R. Hall, A. Lukacs, J. N. Iuliano, G. A. Jones, G. M. Greetham, P. Donaldson, A. Miyawaki, P. J. Tonge, S. R. Meech, *Nat. Chem.*, 2018, **10**, (8), 845
29. G. W. Doorley, D. A. McGovern, M. W. George, M. Towrie, A. W. Parker, J. M. Kelly, S. J. Quinn, *Angew. Chem. Int. Ed.*, 2008, **48**, (1), 123
30. A. W. Parker, C. Y. Lin, M. W. George, M. Towrie, M. K. Kuimova, *J. Phys. Chem. B*, 2010, **114**, (10), 3660
31. P. M. Keane, K. O'Sullivan, F. E. Poynton, B. C. Poulsen, I. V. Sazanovich, M. Towrie, C. J. Cardin, X.-Z. Sun, M. W. George, T. Gunnlaugsson, S. J. Quinn, J. M. Kelly, *Chem. Sci.*, 2020, **11**, (32), 8600
32. J. P. Hall, F. E. Poynton, P. M. Keane, S. P. Gurung, J. A. Brazier, D. J. Cardin, G. Winter, T. Gunnlaugsson, I. V. Sazanovich, M. Towrie, C. J. Cardin, J. M. Kelly, S. J. Quinn, *Nat. Chem.*, 2015, **7**, (12), 961
33. L. A. Hammarback, B. J. Aucott, J. T. W. Bray, I. P. Clark, M. Towrie, A. Robinson, I. J. S. Fairlamb, J. M. Lynam, *J. Am. Chem. Soc.*, 2021, **143**, (3), 1356
34. L. A. Hammarback, I. P. Clark, I. V. Sazanovich, M. Towrie, A. Robinson, F. Clarke, S. Meyer, I. J. S. Fairlamb, J. M. Lynam, *Nat. Catal.*, 2018, **1**, (11), 830
35. N. Põldme, L. O'Reilly, I. Fletcher, J. Portoles, I. V. Sazanovich, M. Towrie, C. Long, J. G. Vos, M. T. Pryce, E. A. Gibson, *Chem. Sci.*, 2019, **10**, (1), 99
36. A. A. Cullen, K. Heintz, L. O'Reilly, C. Long, A. Heise, R. Murphy, J. Karlsson, E. Gibson, G. M. Greetham, M. Towrie, M. T. Pryce, *Front. Chem.*, 2020, **8**, 584060
37. J. B. Eastwood, L. A. Hammarback, M. T. McRobie,

I. P. Clark, M. Towrie, I. J. S. Fairlamb, J. M. Lynam, *Dalt. Trans.*, 2020, **49**, (17), 5463

38. A. Bhattacherjee, M. Sneha, L. Lewis-Borrell, G. Amoruso, T. A. A. Oliver, J. Tyler, I. P. Clark, A. J. Orr-Ewing, *J. Am. Chem. Soc.*, 2021, **143**, (9), 3613
39. A. Bhattacherjee, M. Sneha, L. Lewis-Borrell, O. Tau, I. P. Clark, A. J. Orr-Ewing, *Nat. Commun.*, 2019, **10**, 5152
40. S. Maiti, S. Mitra, C. A. Johnson, K. C. Gronborg, S. Garrett-Roe, P. M. Donaldson, *J. Phys. Chem. Lett.*, 2022, **13**, (34), 8104
41. H. J. Bakker, J. L. Skinner, *Chem. Rev.*, 2010, **110**, (3), 1498
42. P. M. Donaldson, *Anal. Chem.*, 2022, **94**, (51), 17988
43. G. M. Greetham, I. P. Clark, B. Young, R. Fritsch, L. Minnes, N. T. Hunt, M. Towrie, *Appl. Spectrosc.*, 2020, **74**, (6), 720
44. C. P. Howe, G. M. Greetham, B. Procacci, A. W. Parker, N. T. Hunt, *J. Phys. Chem. B*, 2023, **127**, (7), 1586
45. A. P. Hawkins, A. E. Edmeades, C. D. M. Hutchison, M. Towrie, R. F. Howe, G. M. Greetham, P. M. Donaldson, *Chem. Sci.*, 2024, **15**, (10), 3453
46. P. Hamm, M. Zanni, "Concepts and Methods of 2D Infrared Spectroscopy", Cambridge University Press, Cambridge, UK, 2011
47. P. Hamm, M. Lim, R. M. Hochstrasser, *J. Phys. Chem. B*, 1998, **102**, (31), 6123
48. A. Ghosh, J. S. Ostrander, M. T. Zanni, *Chem. Rev.*, 2017, **117**, (16), 10726
49. S. T. Roberts, K. Ramasesha, A. Tokmakoff, *Acc. Chem. Res.*, 2009, **42**, (9), 1239
50. M. D. Fayer, D. E. Moilanen, D. Wong, D. E. Rosenfeld, E. E. Fenn, S. Park, *Acc. Chem. Res.*, 2009, **42**, (9), 1210
51. P. M. Donaldson, *Chem. Sci.*, 2020, **11**, (33), 8862
52. S. Hume, G. Hithell, G. M. Greetham, P. M. Donaldson, M. Towrie, A. W. Parker, M. J. Baker, N. T. Hunt, *Chem. Sci.*, 2019, **10**, (26), 6448
53. R. Fritzsch, P. M. Donaldson, G. M. Greetham, M. Towrie, A. W. Parker, M. J. Baker, N. T. Hunt, *Anal. Chem.*, 2018, **90**, (4), 2732
54. V. C. A. Taylor, D. Tiwari, M. Duchi, P. M. Donaldson, I. P. Clark, D. J. Fermin, T. A. A. Oliver, *J. Phys. Chem. Lett.*, 2018, **9**, (4), 895
55. W. J. Kendrick, M. Jirásek, M. D. Peeks, G. M. Greetham, I. V. Sazanovich, P. M. Donaldson, M. Towrie, A. W. Parker, H. L. Anderson, *Chem. Sci.*, 2020, **11**, (8), 2112
56. C. A. Johnson, A. W. Parker, P. M. Donaldson, S. Garrett-Roe, *J. Chem. Phys.*, 2021, **154**, (13), 134502
57. M. Delor, P. A. Scattergood, I. V. Sazanovich, A. W. Parker, G. M. Greetham, A. J. H. M. Meijer, M. Towrie, J. A. Weinstein, *Science*, 2014, **346**, (6216), 1492
58. P. M. Donaldson, R. F. Howe, A. P. Hawkins, M. Towrie, G. M. Greetham, *J. Chem. Phys.*, 2023, **158**, (11), 114201
59. J. P. Kraack, P. Hamm, *Chem. Rev.*, 2017, **117**, (16), 10623
60. C. Yan, J. Nishida, R. Yuan, M. D. Fayer, *J. Am. Chem. Soc.*, 2016, **138**, (30), 9694
61. J. H. Hack, J. P. Dombrowski, X. Ma, Y. Chen, N. H. C. Lewis, W. B. Carpenter, C. Li, G. A. Voth, H. H. Kung, A. Tokmakoff, *J. Am. Chem. Soc.*, 2021, **143**, (27), 10203
62. P. M. Donaldson, *J. Chem. Phys*., 2024, **160**, 104204
63. S. V. Lepeshkevich, I. V. Sazanovich, M. V. Parkhats, S. N. Gilevich, B. M. Dzhagarov, *Chem. Sci.*, 2021, **12**, (20), 7033
64. J. H. van Wonderen, C. R. Hall, X. Jiang, K. Adamczyk, A. Carof, I. Heisler, S. E. H. Piper, T. A. Clarke, N. J. Watmough, I. V. Sazanovich, M. Towrie, S. R. Meech, J. Blumberger, J. N. Butt, *J. Am. Chem. Soc.*, 2019, **141**, (38), 15190
65. J. H. van Wonderen, K. Adamczyk, X. Wu, X. Jiang, S. E. H. Piper, C. R. Hall, M. J. Edwards, T. A. Clarke, H. Zhang, L. J. C. Jeuken, I. V. Sazanovich, M. Towrie, J. Blumberger, S. R. Meech, J. N. Butt, *Proc. Natl. Acad. Sci.,* 2021, **118**, (39), e2107939118
66. Y. Xiong, A. Vargas Jentzsch, J. W. M. Osterrieth, E. Sezgin, I. V. Sazanovich, K. Reglinski, S. Galiani, A. W. Parker, C. Eggeling, H. L. Anderson, *Chem. Sci.*, 2018, **9**, (11), 3029
67. F. R. Baptista, S. J. Devereux, S. P. Gurung, J. P. Hall, I. V. Sazanovich, M. Towrie, C. J. Cardin, J. A. Brazier, J. M. Kelly, S. J. Quinn, *Chem. Commun.*, 2020, **56**, (67), 9703
68. E. Benazzi, G. H. Summers, F. A. Black, I. V. Sazanovich, I. P. Clark, E. A. Gibson, *Philos. Trans. Royal Soc. A. Math. Phys. Eng. Sci.*, 2019, **377**, (2152), 20180338
69. A. P. Shreve, N. J. Cherepy, R. A. Mathies, *Appl. Spectrosc.*, 1992, **46**, (4), 707
70. T. Tahara, H.-O. Hamaguchi, *Appl. Spectrosc.*, 1993, **47**, (4), 391
71. A. Deffontaine, M. Delhaye, M. Bridoux, 'Pulsed Multichannel Raman Technique', Proceedings of the 2nd International Conference Emil-Warburg Symposium, Bayreuth-Bischofsgrün, Federal Republic of Germany, 3rd–7th June, 1985, "Time-Resolved Vibrational Spectroscopy", eds. A. Laubereau, M. Stockburger, Springer Proceedings in Physics, Vol. 4, Springer-Verlag, Berlin, Heidelberg,

1985, pp. 20–24

72. P. Matousek, M. Towrie, A. Stanley, A. W. Parker, *Appl. Spectrosc.*, 1999, **53**, (12), 1485
73. I. Lezcano-Gonzalez, E. Campbell, A. E. J. Hoffman, M. Bocus, I. V. Sazanovich, M. Towrie, M. Agote-Aran, E. K. Gibson, A. Greenaway, K. De Wispelaere, V. Van Speybroeck, A. M. Beale, *Nat. Mater.*, 2020, **19**, (10), 1081
74. A. R. Neale, D. C. Milan, F. Braga, I. V. Sazanovich, L. J. Hardwick, *ACS Energy Lett.*, 2022, **7**, (8), 2611
75. V. L. Piercy, K. H. Saeed, A. W. Prentice, G. Neri, C. Li, A. M. Gardner, Y. Bai, R. S. Sprick, I. V. Sazanovich, A. I. Cooper, M. J. Rosseinsky, M. A. Zwijnenburg, A. J. Cowan, *J. Phys. Chem. Lett.*, 2021, **12**, (44), 10899
76. F. Provencher, N. Bérubé, A. W. Parker, G. M. Greetham, M. Towrie, C. Hellmann, M. Côté, N. Stingelin, C. Silva, S. C. Hayes, *Nat. Commun.*, 2014, **5**, 4288
77. A. M. Gardner, K. H. Saeed, A. J. Cowan, *Phys. Chem. Chem. Phys.*, 2019, **21**, (23), 12067
78. G. Neri, P. M. Donaldson, A. J. Cowan, *J. Am. Chem. Soc.*, 2017, **139**, (39), 13791
79. G. Neri, J. J. Walsh, G. Teobaldi, P. M. Donaldson, A. J. Cowan, *Nat. Catal.*, 2018, **1**, (12), 952
80. P. M. Donaldson, H. Strzalka, P. Hamm, *Opt. Express*, 2012, **20**, (12), 12761
81. H. Vanselous, P. B. Petersen, *J. Phys. Chem. C*, 2016, **120**, (15), 8175

The Authors

Paul Donaldson is a UKRI Future Leaders Fellow, spectroscopy applications and development group leader at the Central Laser Facility (CLF), UK. Working with the ULTRA facility, Paul's group conducts research into technique development and applications of ultrafast spectroscopy to problems in heterogeneous catalysis, battery and fuel cell science. Paul holds a research Masters and PhD in multidimensional IR techniques (Imperial College London, 2003–2007) followed by postdoctoral research at the University of Zurich, Switzerland. He joined the CLF in 2013. Paul has over 20 years of experience in the techniques of ultrafast spectroscopy.

Igor V. Sazanovich has been a scientist in the CLF ULTRA facility since 2013, delivering experiments for visiting researchers from both academia and industry and developing instrumentation in time resolved spectroscopic techniques, most notably Kerr gated Raman. Igor gained a PhD in time resolved laser spectroscopy applications and instrumentation development at B.I. Stepanov Institute of Physics, Belarus; followed by postdoctoral research in the field at the Institute of Physical Chemistry in Warsaw, Poland; Wageningen University, The Netherlands; Washington University in St. Louis, USA; and the University of Sheffield, UK.

Partha Malakar obtained his PhD from the Department of Chemistry of the Indian Institute of Technology Madras in 2017 and postdoctoral experience with Professor Sanford Ruhman at the Institute of Chemistry of The Hebrew University of Jerusalem, Israel. There, Partha used sub-10 fs pulses to investigate molecular photochemistry and photophysics using transient absorption and impulsive Raman spectroscopy. Partha joined the ULTRA team in 2023 to support user experiments and gain experience with ULTRA's experimental techniques.

Sourav Maiti is currently working as a postdoctoral researcher at the Tata Institute of Fundamental Research (TIFR) Mumbai, India. He worked as a postdoctoral researcher at CLF, Rutherford Appleton Laboratory from 2021–2023. Before joining CLF, he was a postdoctoral researcher at the Delft University of Technology, The Netherlands from 2018–2021. Sourav obtained his PhD in 2018 from Savitribai Phule Pune University, India.

Mike Towrie's research interests are in ultrafast photochemistry, physics and biology, time resolved IR and Raman spectroscopy. Mike is author and co-author on over 250 publications. Since joining the CLF in 1989 his research has centred on development and scientific application of lasers, spectrometers and imaging instrumentation including the Raman Kerr Gate, PIRATE time resolved infrared facilities and STFC and BBSRC funded ULTRA and LIFEtime facilities.

Greg Greetham is the Group Leader of the ULTRA facility at the Rutherford Appleton Laboratory. He began working in high-resolution gas-phase laser spectroscopy with a PhD from the University of Leicester and postdoctoral research at ETH Zurich. He moved to industry to develop femtosecond lasers at Amplitude. Greg has been at the CLF since 2005, applying state-of-the-art femtosecond laser systems to spectroscopy technique development and supporting scientific research facilities serving academia and industry across the UK and internationally.